

Open-radiomics: A Collection of Standardized Datasets and a Technical Protocol for Reproducible Radiomics Machine Learning Pipelines

Khashayar Namdar^{1,2,4,8,9}, Matthias W. Wagner^{1,2,3,5}, Birgit B. Ertl-Wagner^{1,2,3}, Farzad Khalvati^{1,2,3,4,6,7,8}

Affiliations:

1. Department of Diagnostic Imaging & Image-Guided Therapy, The Hospital for Sick Children (SickKids), Toronto, ON, Canada
2. Neurosciences & Mental Health Research Program, SickKids Research Institute, Toronto, ON, Canada
3. Department of Medical Imaging, University of Toronto, Toronto, ON, Canada
4. Institute of Medical Science, University of Toronto, Toronto, ON, Canada
5. Department of Diagnostic and Interventional Neuroradiology, University Hospital Augsburg, Germany
6. Department of Computer Science, University of Toronto, Toronto, ON, Canada
7. Department of Mechanical and Industrial Engineering, University of Toronto, Toronto, ON, Canada
8. Vector Institute, Toronto, ON, Canada
9. NVIDIA Deep Learning Institute, Austin, TX, United States

Abstract

Purpose: As an important branch of machine learning pipelines in medical imaging, radiomics faces two major challenges namely reproducibility and accessibility. In this work, we introduce open-radiomics, a set of radiomics datasets along with a comprehensive radiomics pipeline based on our proposed technical protocol to investigate the effects of radiomics feature extraction on the reproducibility of the results.

Materials and Methods: Experiments are conducted on BraTS 2020 open-source Magnetic Resonance Imaging (MRI) dataset that includes 369 adult patients with brain tumors (76 low-grade glioma (LGG), and 293 high-grade glioma (HGG)). Using PyRadiomics library for LGG vs. HGG classification, 288 radiomics datasets are formed; the combinations of 4 MRI sequences, 3 binWidths, 6 image normalization methods, and 4 tumor subregions.

Random Forest classifiers were used, and for each radiomics dataset the training-validation-test (60%/20%/20%) experiment with different data splits and model random states was repeated 100 times (28,800 test results) and Area Under Receiver Operating Characteristic Curve (AUC) was calculated.

Results: Unlike binWidth and image normalization, tumor subregion and imaging sequence significantly affected performance of the models. T1 contrast-enhanced sequence and the union of necrotic and the non-enhancing tumor core subregions resulted in the highest AUCs (average test AUC 0.951, 95% confidence interval of (0.949, 0.952)). Although 28 settings and data splits yielded test AUC of 1, they were irreproducible.

Conclusion: Our experiments demonstrate the sources of variability in radiomics pipelines (e.g., tumor subregion) can have a significant impact on the results, which may lead to superficial perfect performances that are irreproducible.

Keywords: radiomics, open-source, dataset, brain cancer, reproducibility

Introduction

Artificial Intelligence (AI) has found its applications across different fields, and medical imaging is one of the high-potential areas where AI solutions are promising [1], [2]. Machine Learning (ML) is a subset of AI with tools for classification, regression, and decision-making, with many applications for medical imaging data [3]. ML algorithms in medical imaging fulfill tasks such as region of interest (ROI) segmentation and classification, and they are used as building blocks of AI-based pipelines for diagnosis, prognosis, and therapeutic assessments.

Deep Learning (DL) is a branch of ML where multiple-layer Neural Networks (NNs) are utilized at its core. Currently, AI-based segmentation is usually done using DL algorithms. However, for ML-based classification of medical imaging data, DL has a conventional competitor namely radiomics. The suffix “omics” refers to large-scale data derived to understand a biological perspective, such as genomics in Genetics [4]. Radiomics is a large set of manually-defined features to study ROIs in Radiology. From the Data Science point of view, radiomics provides a mapping, i.e., converting images into tabular data. Usually, radiomics studies start with image annotation, where 2D/3D ROIs are segmented. Each radiomic feature is the result of applying a distinct and predefined equation to the ROI. Once the radiomic features are extracted, any ML classifier capable of handling tabular data, such as Random Forests (RF) [5], can be used to perform the classification task.

In comparison to DL, radiomics may offer a higher degree of explainability since its features are derived using transparent equations. However, there are multiple sources of variability impacting radiomics generalizability and reproducibility [6]. Radiomic features are sensitive to any form of change in ROIs (i.e., if intensity values of image pixels/voxels within an ROI are manipulated). Different vendors, imaging device settings, imaging protocols, contouring discrepancy (known as intra- and inter-reader variability), image normalization, and radiomics extraction settings might result in variation in radiomics results. Insufficient technical details, such as data split information, and lack of openness to the data and codes are other obstacles to having reproducible radiomics research. Depending on the source of the variability, addressing the issue might be infeasible in a given study. An example is tackling intra- and inter-reader variability in a fixed dataset of radiology images and ROI segmentations, without further information about the reader. Nevertheless, all these sources of variability create a demand for a proper statistical approach for measuring the randomness and hence, the reliability of radiomics studies. Radiomics studies often lack systematic randomness measurements. Thus, in this research, the aim is to provide an open-source radiomics dataset along with a baseline classification pipeline. We also propose a technical protocol for radiomics pipelines, targeting reproducible radiomics-based classification models.

In this research, we use the BraTS 2020 [7] [8] [9], an open-source multimodal Magnetic Resonance Imaging (MRI) dataset for brain tumor segmentation. Because BraTS is primarily a segmentation dataset, the majority of articles in the literature are dedicated to contouring brain tumors [7], [9], [10]. Dequidt et al. [11] used BraTS 2018 to conduct a radiomics-based low-grade glioma (LGG) vs. high-grade glioma (HGG) classification task. Five expert radiologists labeled the tumors based on World Health Organization (WHO) standards, which enabled them to compare their model against another set of ground truths in addition to the BraTS labels. They extracted a limited set of radiomic features (51 features for each MRI sequence), used Support Vector Machines (SVM) [12] as the classifier with a 5-fold cross-validation for hyperparameter optimization, and achieved 84.1% accuracy with reference to the BraTS ground truths.

Coupet et al. used BraTS 2020 as one of the datasets to train their models for healthy vs. glioma classification [13]. Polly et al. applied Otsu thresholding [14] to the images, used k-means for segmentation, Discrete Wavelet Transform (DWT) for feature extraction, and Principal Component Analysis (PCA) for dimensionality reduction, followed by SVM for a two-stage classification: abnormal vs. normal and then HGG vs. LGG. They achieve 99% accuracy on a small and balanced subset (50 HGG and 50 LGG) of BraTS 2017 and BraTS 2013 datasets, with a one-time data split approach.

In this paper, using BraTS 2020 dataset, we propose a comprehensive approach to investigating the effect of image normalization, the most impactful radiomics feature extraction hyperparameter (binWidth), imaging sequence, and tumor subregion on a radiomics-based tumor type classification pipeline.

Related work

Previous studies on the pLGG classification using ML are limited. Nonetheless, multiple impactful clinical studies have been conducted. Bag et al. provided comprehensive details about the radiohistogenomics of pLGG, and how different factors contribute to risk stratification of the patients [15]. They identified five genetic profile, location, age at presentation, and histology as the decisive features for pLGG phenotype risk assessment. They also listed BRAF fusion and BRAF V600E point mutation (BRAF mutation) among the common gene alterations in pLGG (i.e., pLGG molecular subtype), and illustrate how the two subtypes are different in term of tumor location. In their study, while 75% of the BRAF Fusion cases were located in cerebellum, the rate for BRAF mutation was only 5%. In contrast, majority of BRAF mutation cases were observed in cerebral hemispheres (56%). As a consequence, BRAF fusion tumors are often surgically resectable, leading to excellent overall survival and low progression rates [16].

Wagner et al. used radiomics to conduct pretherapeutic differentiation of BRAF-mutated and BRAF-fused tumors [17]. In their bi-institutional retrospective study, T2 Fluid-Attenuated Inversion Recovery (FLAIR) MR images of 115 pediatric patients from 2 children's hospitals were analyzed. They extracted radiomics features from the ROIs that a pediatric neuroradiologist provided, and used RF as the binary classifier. They evaluated the models using a 4-fold cross validation on 94 patients from one institute and conducted a one-time external validation on the remaining 21 patients from the second hospital. They provided the receiver operating characteristic (ROC) curves of the models and achieved an average area under the ROC curve (AUROC) of 0.75 on the internal cohort and an AUROC of 0.85 on the external cohort. Their statistical analysis showed location (supra- versus infratentorial) and age were significant predictors of BRAF status on the first cohort. Additionally, the average AUROC was improved to 0.77 when age and location were appended to the radiomics features.

In a separate study on a larger bi-institutional dataset of 251 pLGG FLAIR MR images, Wagner et al. conducted the dataset size sensitivity analysis [18]. They showed data splits and model initialization impose randomness to the performance of the ML classifiers which impacts the results in two aspects, namely average AUROC and variance of the AUROCs. They confirmed the scale of the dataset size was reliable to train robust pipelines, but an individual global model could be biased. With only 60% of the training data, they achieved comparable results to those of models that used the entire training set, with an average AUROC of 0.83 compared to 0.85.

Haldar et al. retrospectively studied a dataset of 157 pLGG patients from the Children's Hospital of Philadelphia (CHOP), and utilized a conventional unsupervised ML algorithm to classify the subjects [19]. In unsupervised ML, the models are trained to find patterns in the data without considering the labels which makes this framework appropriate for unlabelled data. In the context of classification, it is common to use unsupervised ML for data clustering. However, data clusters and labels, in this case pLGG subtypes, may not agree, and thus supervised ML is preferred. Conforming to the clustering approach, Haldar et al. employed PCA followed by K-means algorithm to assign the patient images into three subgroups. Using Kruskal-Wallis test, they demonstrated that the distribution of tumor histology and location among the three imaging clusters was different. Although PCA is sensitive to outliers and combination of the statistical analysis and unsupervised learning has a weak predictive power compared to supervised learning, the study is another evidence for the importance of location in pLGG subtype identification.

Korfiatis et al. reviewed ML approaches, including DL, for predicting molecular markers from MRI [20]. They provided a summary of the benchmark models for different datasets of brain glioma, such as Medulloblastoma and Glioblastoma. They highlighted that DL had significantly improved prediction of markers for gliomas but lacked feature interpretability. Nevertheless, they did not provide any specific study on pLGG or tumor location.

Xu et al. analyzed a dataset of 113 pLGG patients (43 BRAF V600E mutations versus 70 cases of other subtypes) using radiomics features to identify BRAF mutations [21]. They conducted a one-time train-test splitting with the ratio of 70/30 and employed a 5-fold cross-validation to find the best setting for their pipeline using the training cohort. Multiple classifiers were evaluated, and RF outperformed all. They achieved an average training AUROC of 0.72, with 95 % confidence interval (CI), (0.602, 0.831), and a test AUROC of 0.875. Although the data splitting approach may result in irreproducible AUROCs, their conclusions are remarkable. Tumor location (supratentorial versus infratentorial) was a significant predictor of BRAF mutation and when combined with radiomics, it improved the average training AUROC to 0.754 with 95% CI of (0.645, 0.844) and the test AUROC to 0.934. Additionally, tumor location side (left versus right) was studied, and it was not a significant predictor of BRAF mutation.

Materials and Methods

While there is annotated open-source medical imaging data, the extracted radiomics features are not usually available. Thus, each researcher must choose the appropriate tools/libraries and settings to extract the features. Consequently, radiomics studies are often conducted on small internal datasets with a narrowed-down selection of hyperparameters for extracting the features. Open-radiomics (<https://openradiomics.org>) is our initiative for open-source large-scale radiomics datasets where we provide AI-ready tabular datasets along with baselines.

One of the sources of variability in radiomics research is the discrepancy between the feature extraction software and packages used across the studies. Multiple options are available to the research community for radiomics feature extraction [22]. Nonetheless, their back-ends might be different (e.g., different default settings or numerical precision), leading to irreproducibility of radiomics research. We will use PyRadiomics [23], which is widely used and supported by a large and established community. It should be highlighted that PyRadiomics-based packages,

such as the Slicer Radiomics add-on module for 3D Slicer software (<https://www.slicer.org/>) [24] might mask some features of PyRadiomics, resulting in suboptimal feature extraction.

Dataset

The dataset is a collection of multisequence MRIs, including T1-weighted (T1), gadolinium-based contrast agent enhanced T1-weighted (T1CE), T2-weighted (T2), and FLAIR sequences. The training cohort of BraTS 2020 is the data applicable to our research because its ground truth (GT) ROI segmentations are available. The cohort includes 369 adult patients with brain tumors, of which 76 cases are LGG, and 293 are HGG tumors. The images are all co-registered to the SRI24 atlas [25], skull stripped, resampled to 1 mm^3 , and their size is unified to $155 \times 240 \times 240$ voxels. We acknowledge that there is a discrepancy in the definition of LGG and HGG between BraTS and WHO [11]. In this paper, we follow the binary grading system (HGG vs. LGG) provided by BraTS.

BraTS 2012-2016 included four tumor subregions, labeled 1-4. The necrotic (NCR), and the non-enhancing (NET) tumor core were labeled as 1 and 3, respectively. Label 2 corresponded to the peritumoral edematous/invaded tissue (ED), and active tumor (AT) was labeled as 4. Since BraTS 2017, NET and NCR are combined, and label 3 is removed from the annotations. Figure 1 depicts one slice of an image volume along with its corresponding segmentation mask. We analyze the whole tumor (all four subregions combined), AT, ED, and the union of NET and NCR (NETnNCR), in separate scenarios.

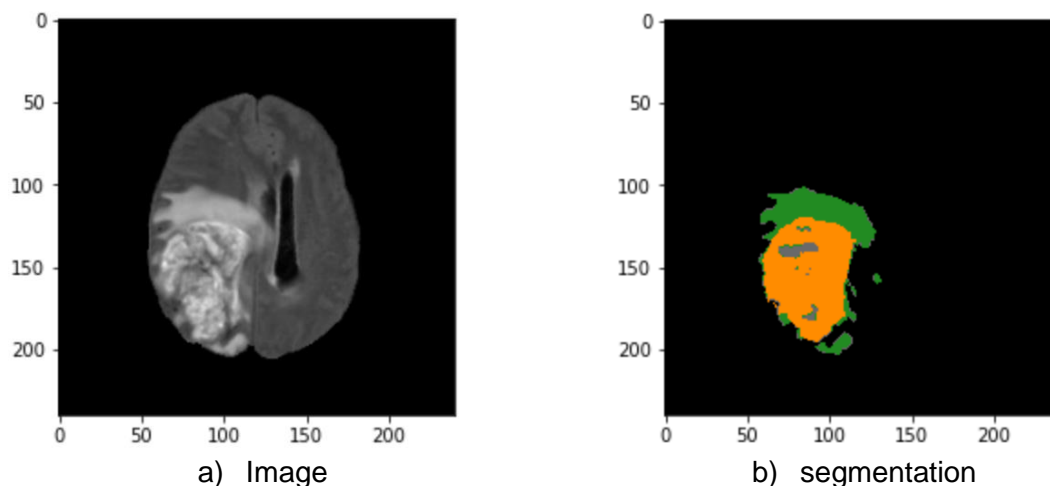


Figure 1: An example image (the FLAIR sequence) and its corresponding segmentation mask. The orange area is AT, the green area is ED, and the gray parts are NETnNCR

PyRadiomics Library

Radiomics feature extraction using PyRadiomics is a sophisticated task, and there are technical details to be considered. Installation of the trimesh python package is essential for radiomic feature extraction (Can be fulfilled through `pip install trimesh`) to ensure calculation of all feature categories.

In general, radiomics studies might be 2D or 3D. A 2D analysis is used when the imaging method is 2D, such as X-Ray. However, when 3D images are accessible, 2D and 3D radiomics analyses are both possible. If the 2D approach is utilized with 3D images, often the analysis is done on the largest tumor 2D cross-section. In the case of 3D analyses, such as this project, enabling the full set feature extraction forces the library to extract 2D Local Binary Pattern (LBP) features [26] in addition to the 3D LBP features (see Appendix A). In this research, we included 2D LBP features, and thus a full set of 1,710 features were extracted for each ROI.

PyRadiomics has multiple hyperparameters that affect the feature extraction procedure (<https://pyradiomics.readthedocs.io/en/latest/customization.html>). One of the most important is `binWidth`, which has been studied in the literature extensively [27]. `binWidth` determines the bin size which is needed to create histograms used for discretizing gray levels in the image, and thus it affects all features except the shape features which are independent of pixel/voxel intensities. The default value of `binWidth` in PyRadiomics is 25. In this research, in addition to 25, we examine 35 and 15 to see how they affect the results. All other hyperparameters are set to their default values (<https://pyradiomics.readthedocs.io/en/latest/customization.html>).

Image normalization

Image normalization plays an important role in ML pipelines, which can influence radiomics significantly. We implemented histogram equalization [28], z-score [29], gamma [30], and minmax [31] image normalization methods and incorporated them into our 3D analyses. As the coefficients of our gamma normalization, we explored 0.5 and 1.5, and the minmax normalization clipped voxel values of the image volumes between 0 and 1. All the normalization methods were applied to the image volumes, not the ROIs. We did not investigate ROI normalization in this research because it would increase the computational load. Nonetheless, it can be studied in the future.

Classification pipeline

Once feature extraction is completed, the classification modules can be designed and implemented. With the default settings of PyRadiomics, each dataset has a group of diagnostics features (e.g., python version, simple itk version, etc.), which will not contain differentiative information, and thus we filter them.

We employ a repetitive approach to measure randomness of our radiomics-based ML classification pipeline, which is illustrated in Figure 2. We suggest the same approach be utilized in any radiomics study. We repeat our evaluations on the test sets N times. In this research, N is set to 100. In the external for loop with N repetitions, in each iteration we randomly split our data into test ($p\%$) and development (dev) sets. In this research, p was set to 20%. In the next step, a feature filtration algorithm is trained on the dev set and applied to the test set to randomly drop one of the features in pairs with a correlation coefficient above 0.95. Another layer of feature selection is Near-zero Variance (NZV) filtration. We train an algorithm on the dev set and apply it to the test cohort to remove any feature with a variance lower than 0.05. The last step of feature manipulation is a MinMax scaler which learns the transformations from the dev set and applies them to the test.

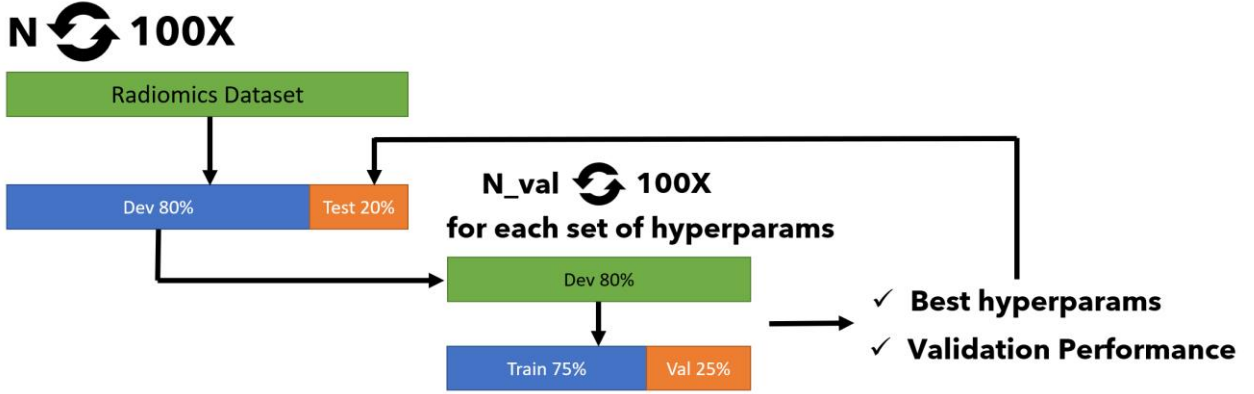


Figure 2: The repetitive classification approach

RF models are explainable and differentiative when applied to radiomics [17][32], and thus we chose them as our baseline classifiers. We defined a grid space for our classifier which is described in appendix B. For each combination of the hyperparameters in the grid space, we conduct N_{val} experiments (internal for loop). In this research, N_{val} was set to 100. In each experiment, the dev set is randomly split into training and validation ($p_{val}\%$) cohorts. In this research, p_{val} is set to 25%. An instance of the classifier with the proposed hyperparameters is trained using the training set, and evaluated on the validation set based on the random split. While we use AUROC as our evaluation metric, any other criterion, such as accuracy, might be utilized. Nonetheless, not all metrics are suitable for imbalanced datasets and medical contexts [33]. Once the N_{val} experiments are completed for the whole grid space, the best hyperparameter set is derived based on the highest average AUROC. To measure the validation performance, instances of models with the best hyperparameter set are trained and validated N_{val} times on random data splits with $p_{val}\%$ ratio. Average AUROC is considered to be the validation performance of the models. In the final step, an instance of the model with the best hyperparameters is trained on the entire dev set and evaluated on the test cohort. As it was mentioned, the whole process is repeated N times, and thus we have N test AUROCs as well as N validations AUROC.

Data management and other technical concerns such as deriving feature importance are discussed in appendices C and D, respectively. Table 1. includes the Open-radiomics technical protocol, and the settings for this study are provided appendix E.

Table 1. Open-radiomics technical research protocol

	Technical consideration	Notes
1	Sources of variability for the research must be identified	
2	The sources of variability, whose effect will be measured, should be highlighted	
3	Authors should mention which tool was used for radiomics extraction	PyRadiomics is recommended
4	It must be confirmed all the required libraries were installed	In the case of PyRadiomics, the trimesh python library is required
5	All possible features should be extracted	Full set feature extraction is recommended. In the case of PyRadiomics, <code>extractor.enableAllImageTypes()</code> and <code>extractor.enableAllFeatures()</code> should be applied

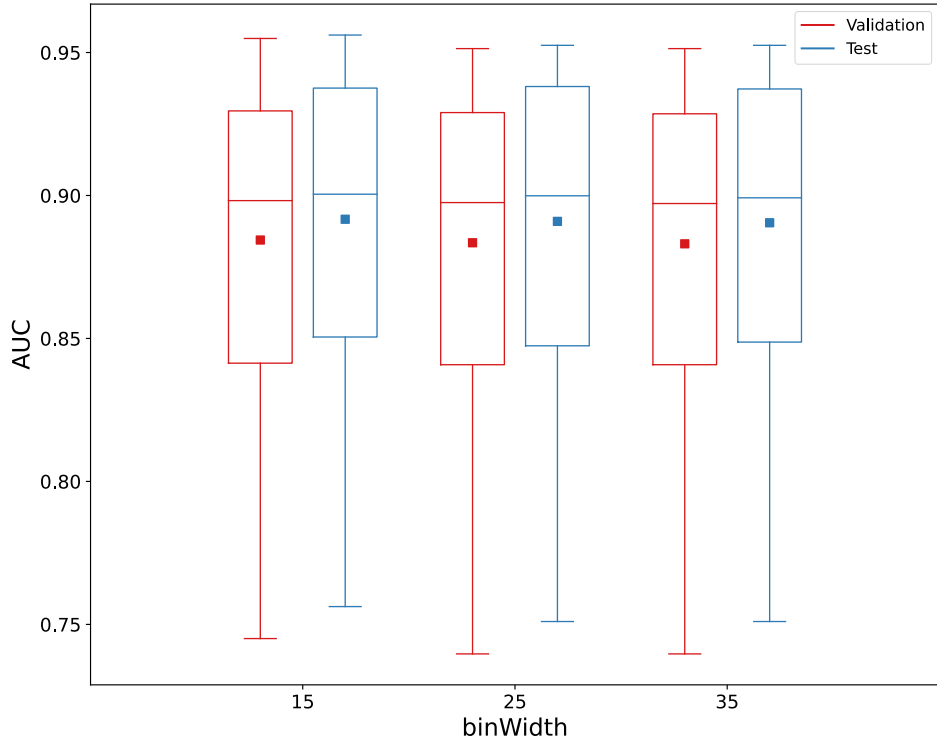
6	It should be highlighted whether the study was 2D or 3D	In the case of 2D radiomics study on volumetric data, detailed processes of deriving ROIs should be included
7	The list of the extracted radiomics feature names must be provided in the supplementary materials	Providing the full list improved reproducibility of the research
8	A sample of the diagnostics features must be provided in the supplementary materials	Diagnostic features provide information about the environment that was used for feature extraction, improving repeatability and reproducibility of the research
9	The data split and model initialization must be repeated	With the small-size datasets, repeated train/validation/test splitting is recommended. If the number of repeats is low, e.g., 5-fold cross-validation, the training and validation indices should be provided
10	It must be highlighted if the pipeline included feature engineering	Any feature filtration, feature selection, or feature normalization technique should be learned from training or development sets and applied to the test set. Dataset-wise feature engineering may impact generalizability of the pipeline and thus lead to bias
11	The model, hyperparameter grid space, and evaluation metric(s) must be discussed in detailed	
12	It should be highlighted if the final model was trained on the development set or the training cohort	Retraining the model using the development set and the optimized hyperparameters is an effective approach for boosting the performance on small datasets. It can result in superior test performance compared to validation.
13	It is highly recommended the dataset (extracted radiomics features and the ground truth labels) be open-sourced	
14	The details of how the top-performing radiomics features were identified must be provided	

Results

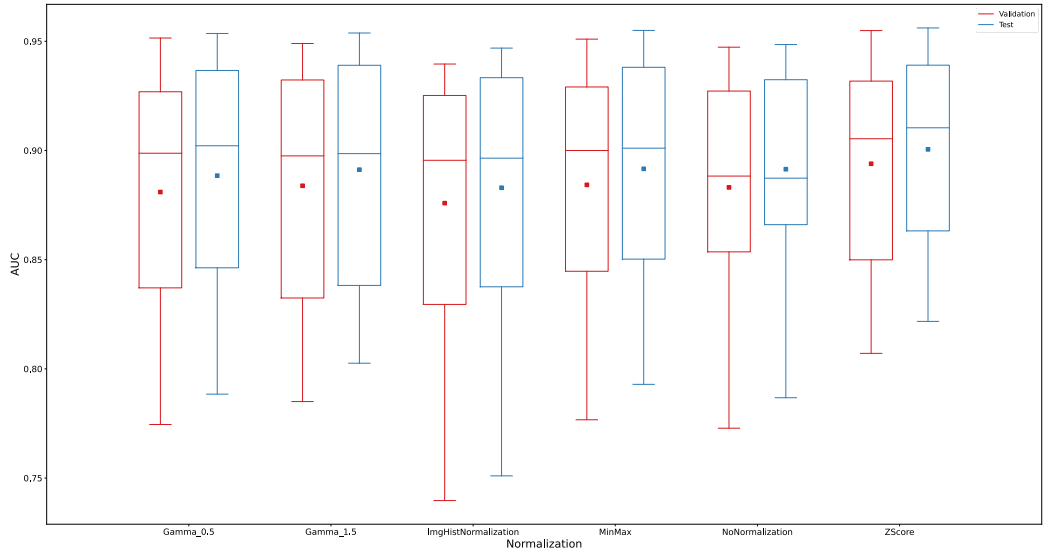
Classification Performance

Figure 3 illustrates the effect of the four sources of variability on the AUROC performance of the classifiers, for validation and test cohorts. It should be highlighted the highest AUROC might not be achieved with the combination of the best image normalization, binWidth, tumor subregion, and MRI sequence. Our approach is repetition-based and can be considered as a stochastic or random process, whose output is individual AUROCs. We achieve the highest average test AUROC performance (0.956 ± 0.033) across the 100 experiments on T1CE, for NETnNCR subregion, with ZScore normalization, and with binWidth of 15. The second and the third top-performing datasets (mean test AUROCs of 0.955 ± 0.030 and 0.954 ± 0.032 , respectively) had the same setting except for their image normalization, which was MinMax, and Gamma 1.5, respectively. Figure 4 depicts how the top feature (lbp-3D-k_glszm_HighGrayLevelZoneEmphasis) differentiates the HGG and LGG examples on the top-performing dataset.

a)



b)



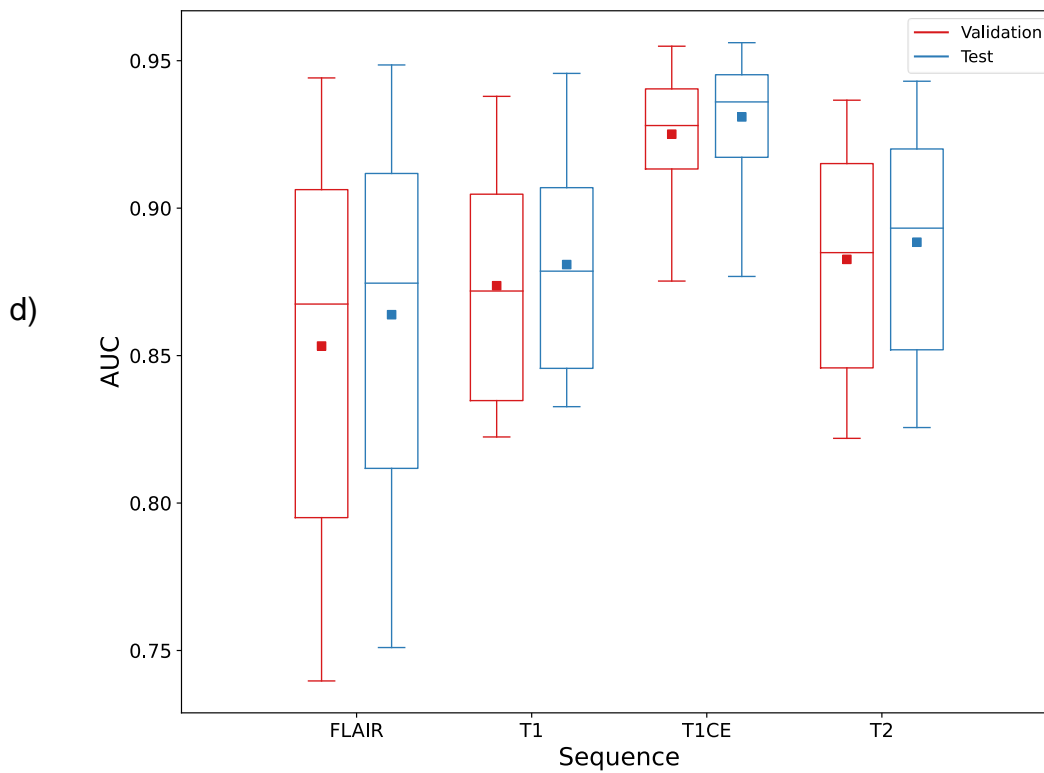
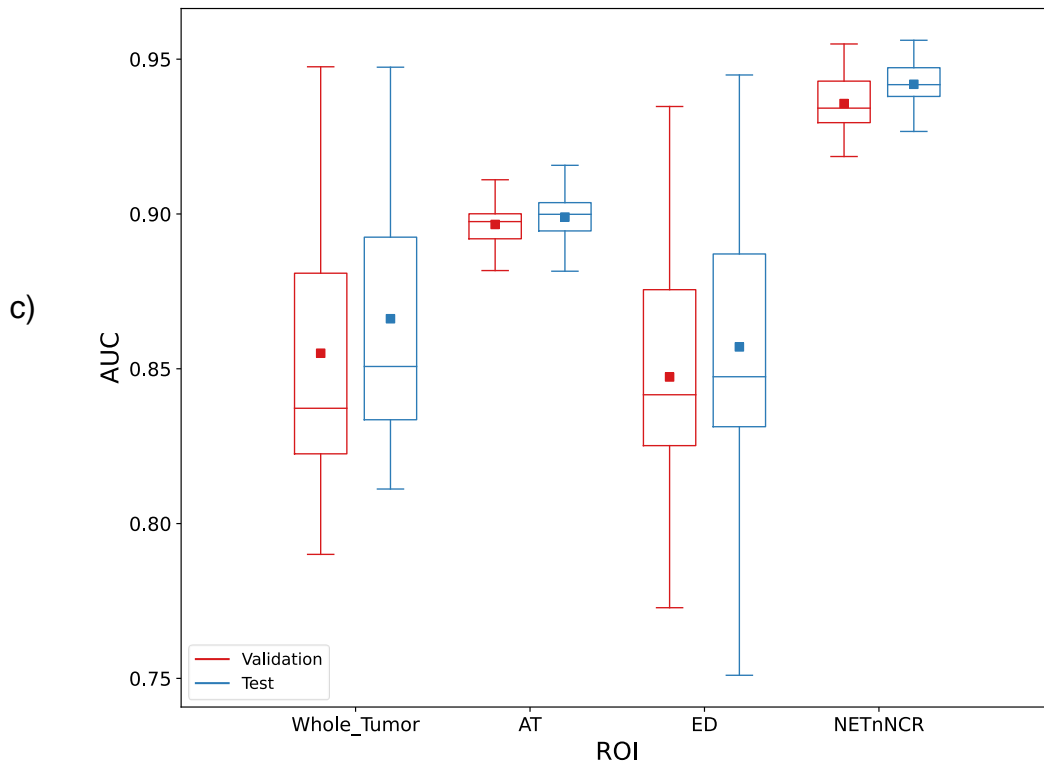


Figure 3: Effect of the studied factors on AUROC performance of the classifiers: a) binWidth b) image normalization c) ROI subregion d) MRI sequence

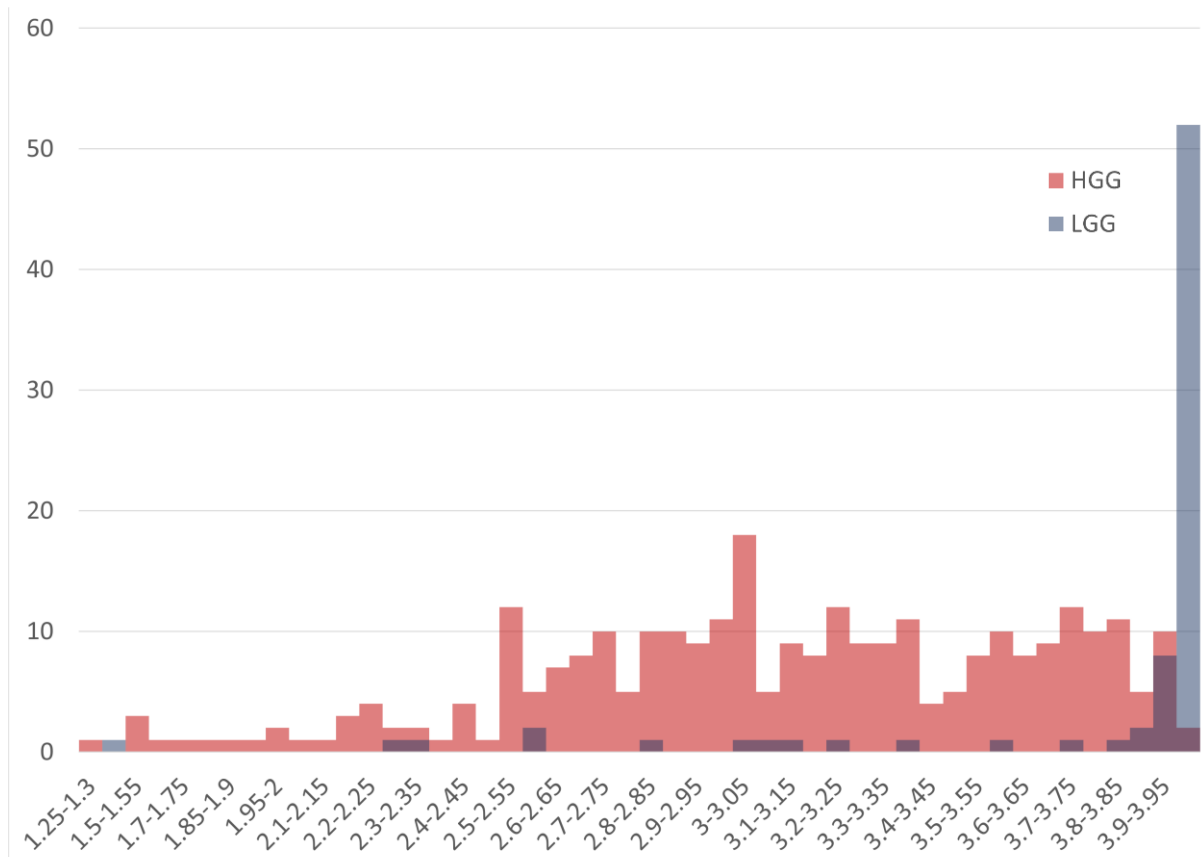


Figure 4: Histograms of the top feature on the top dataset: The horizontal axis represents bins of the feature values, and the vertical axis shows the number of ROIs with values in each bin

It is important to note that the boxplots in Figure 3 represent the range of average AUROCs. Hence, the maximum test performance of NETnNCR in Figure 3-c (AUROCs = 0.956) is itself an average of 100 experiments. Thus, there are multiple experiments in which we achieve very high AUROCs close or equal to 1.00. Obviously, such high results are not reproducible. Along with the mean for each dataset, we also captured min, median, max, and first and third quartile of the AUROC performances. In 140 datasets out of 288, the highest achievable AUROC was above 0.99. In 28 cases, including T1CE, ZScore normalization, whole tumor classification, binWidth15, we reached to AUROC of 1.00. Nonetheless, our results prove that AUROC of 1.00 for the whole tumor classification is extremely irreproducible. Figure 5 illustrates the range of AUROC performance of the top-ten datasets.

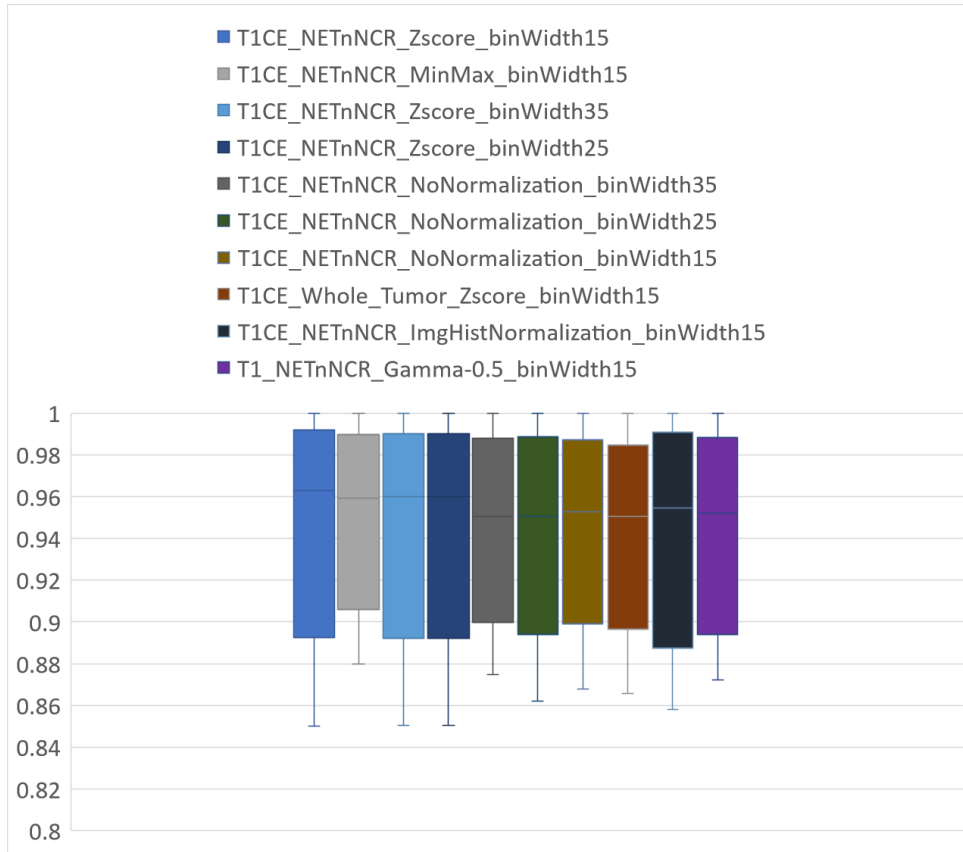


Figure 5: The 10 top-performing datasets

Discussion

We investigated the effect of PyRadiomics binWidth, image normalization method, ROI subregion, and the MRI sequence on our radiomics-based ML brain tumor type classification pipeline. We first investigated the configurations where the feature extraction failed altogether (see Appendix F). Next, we studied the effects of the studied factors on the classification performance.

Feature Extraction Failure

For BraTS 2020, considering the number of failed radiomic feature extractions (696 out of 106,272), the optimal PyRadiomics binWidth appears to be 25, which is the default. While the type of image normalization does not make a difference (348 failed cases), lacking normalization is exacerbating (445 cases). The chance of having a successful feature extraction is increased if the subregion is bigger and more convex. Hence, the best case is whole tumor classification (48 failed cases), and the worst case is AT (1952 cases). While the difference between the sequences is marginal, T1 and T1CE are the best and worst sequences, respectively (535 vs 556 cases).

Classification Performance

Overall, binWidth does not make a tangible difference (average test AUROCs 0.892, 0.891, 0.890 for binWidth of 15, 25, and 35, respectively). Among the image normalization techniques we examined, ZScore slightly improved the average performance of the models (AUROC = 0.901). It also decreased the variance of the test AUROCs (average standard deviation (SD) 0.042), which is another desirable point. Our results suggest the true potential of radiomics might not be exploited for the whole tumor classification of BraTS 2020. In the case of ED, we observed the highest AUROC variances (SD=0.055). In contrast, the models are surprisingly accurate and precise for NETnNCR classification of HGG and LGG tumors with an average test AUROC of 0.942. While for AT, the average test AUROCs is 0.899, the variance is low (SD=0.010), and thus the results are reproducible. Among the four MRI sequences, T1CE surpasses the others significantly (AUROC=0.931), and the lowest AUROC performances come out of FLAIR (AUROC=0.864).

Top Ranking Feature

Except for the shape and first-order features, explaining the details and physical meaning of radiomics features is not straightforward. Radiomics includes multiple groups of features, which are described in the Image Biomarker Standardization Initiative (IBSI) [34]. In our experiments, lbp-3D-k_glszm_HighGrayLevelZoneEmphasis radiomic feature appeared most frequently among the top features. LBPs are operators that label pixels (or voxels, in the case of 3D ROIs) of images based on thresholding their neighbor points [26]. To form the lbp-3D-k, PyRadiomics extracts the spherical kurtosis image using the `scipy.stats.kurtosis` function [35], and applies the LBP operator to it. Kurtosis is defined as the fourth central moment times inverse of the square of the variance, and the kurtosis image corresponds to calculating kurtosis for every voxel. In radiomics, Gray Level Size Zone Matrix (GLSZM) is used for quantifying gray level zones in images. Gray level zones are defined as the number of connected voxels with similar gray-level intensities. High Gray Level Zone Emphasis (HGLZE), which is formulated as Eq. 1, represents a measurement of the distribution of the higher gray-level values. Higher HGLZE means the ROI contains a greater proportion of higher gray-level values and size zones.

$$HGLZE = \frac{\sum_{i=1}^{N_g} \sum_{j=1}^{N_s} \frac{P(i,j)}{i^2}}{N_z} \quad \text{Eq. 1}$$

In Eq. 1., N_g and N_s correspond to the number of discrete intensity values, and the number of discrete zone sizes in the image, respectively. N_z is the number of zones in the ROI, and $P_{(i,j)}$ is the size zone matrix.

Conclusion

In this research, we proposed a research protocol for radiomics-based ML pipelines to improve reproducibility. We extracted and open-sourced a large series of tabular radiomics datasets based on the BraTS 2020 dataset that enables multiple opportunities for radiomics research. We established a reproducible baseline for the open-radiomics datasets, and studied the effect of PyRadiomics binWidth, image

normalization, ROI subregion, and the MRI sequence as four sources of variability on the performance of the radiomics pipeline.

Our experiments demonstrated the default binWidth increases the chance of a successful ROI feature extraction, while it has no effect on the generalizability of the model. NETnNCR ROI subregion is associated with the highest-performing models, and AT ranks second. However, ED and whole tumor classifications struggle to achieve comparable performance. We found T1CE and FLAIR to be the best and worst sequences, respectively. While these results may be specific to BraTS dataset, the protocol can be followed to generate reliable and reproducible radiomics results for any given dataset.

Acknowledgement

This research has been made possible with the financial support of the Canadian Institutes of Health Research (CIHR) (Funding Reference Number: 184015)

References

- [1] X. Liu *et al.*, “Application of radiomic MRI quantitative features in diagnosis of combined hepatocellular-cholangiocarcinoma, cholangiocarcinoma and hepatocellular carcinoma using machine learning,” 2019.
- [2] X. Liu *et al.*, “Can machine learning radiomics provide pre-operative differentiation of combined hepatocellular cholangiocarcinoma from hepatocellular carcinoma and cholangiocarcinoma to inform optimal treatment planning?,” *Eur. Radiol.*, 2020, doi: 10.1007/s00330-020-07119-7.
- [3] M. W. Wagner, K. Namdar, A. Biswas, S. Monah, F. Khalvati, and B. B. Ertl-Wagner, “Radiomics, machine learning, and artificial intelligence—what the neuroradiologist needs to know,” *Neuroradiology*, vol. 63, no. 12, pp. 1957–1967, 2021, doi: 10.1007/s00234-021-02813-9.
- [4] S. P. Yadav, “The wholeness in suffix -omics, -omes, and the word om.,” *J. Biomol. Tech.*, vol. 18, no. 5, p. 277, Dec. 2007.
- [5] L. Breiman, “Random Forests,” *Mach. Learn.*, vol. 45, no. 1, pp. 5–32, 2001.
- [6] J. E. Park, S. Y. Park, H. J. Kim, and H. S. Kim, “Reproducibility and generalizability in radiomics modeling: Possible strategies in radiologic and statistical perspectives,” *Korean J. Radiol.*, vol. 20, no. 7, pp. 1124–1137, 2019, doi: 10.3348/kjr.2018.0070.
- [7] B. H. Menze *et al.*, “The Multimodal Brain Tumor Image Segmentation Benchmark (BRATS).,” *IEEE Trans. Med. Imaging*, vol. 34, no. 10, pp. 1993–2024, Oct. 2015, doi: 10.1109/TMI.2014.2377694.
- [8] S. Bakas *et al.*, “Advancing The Cancer Genome Atlas glioma MRI collections with expert segmentation labels and radiomic features.,” *Sci. data*, vol. 4, p. 170117, Sep. 2017, doi: 10.1038/sdata.2017.117.
- [9] S. Bakas *et al.*, “Identifying the Best Machine Learning Algorithms for Brain Tumor Segmentation, Progression Assessment, and Overall Survival Prediction in the BRATS Challenge.” 2018.
- [10] U. Baid *et al.*, “The RSNA-ASNR-MICCAI BraTS 2021 Benchmark on Brain Tumor Segmentation and Radiogenomic Classification.” 2021.
- [11] P. Dequidt *et al.*, “Exploring Radiologic Criteria for Glioma Grade Classification

- on the BraTS Dataset,” *IRBM*, vol. 42, no. 6, pp. 407–414, 2021, doi: <https://doi.org/10.1016/j.irbm.2021.04.003>.
- [12] M. A. Hearst, S. T. Dumais, E. Osuna, J. Platt, and B. Scholkopf, “Support vector machines,” *IEEE Intell. Syst. their Appl.*, vol. 13, no. 4, pp. 18–28, 1998.
- [13] M. Coupet *et al.*, “A multi-sequences MRI deep framework study applied to glioma classification,” *Multimed. Tools Appl.*, 2022, doi: 10.1007/s11042-022-12316-1.
- [14] D. Liu and J. Yu, “Otsu Method and K-means,” in *2009 Ninth International Conference on Hybrid Intelligent Systems*, 2009, vol. 1, pp. 344–349, doi: 10.1109/HIS.2009.74.
- [15] A. K. Bag, J. Chiang, and Z. Patay, “Radiohistogenomics of pediatric low-grade neuroepithelial tumors.,” *Neuroradiology*, vol. 63, no. 8, pp. 1185–1213, Aug. 2021, doi: 10.1007/s00234-021-02691-1.
- [16] S. Ryall, U. Tabori, and C. Hawkins, “Pediatric low-grade glioma in the era of molecular diagnostics,” *Acta Neuropathol. Commun.*, vol. 8, no. 1, pp. 1–22, 2020, doi: 10.1186/s40478-020-00902-z.
- [17] M. W. Wagner *et al.*, “Radiomics of pediatric low grade gliomas: toward a pretherapeutic differentiation of BRAF-mutated and BRAF-fused tumors,” *Am. J. Neuroradiol.*, 2021.
- [18] M. Wagner *et al.*, “Dataset Size Sensitivity Analysis of Machine Learning Classifiers to Differentiate Molecular Markers of Pediatric Low-Grade Gliomas Based on MRI.” Research Square, 2021, doi: 10.21203/rs.3.rs-883606/v1.
- [19] D. Haldar *et al.*, “Unsupervised machine learning using K-means identifies radiomic subgroups of pediatric low-grade gliomas that correlate with key molecular markers.,” *Neoplasia*, vol. 36, p. 100869, Feb. 2023, doi: 10.1016/j.neo.2022.100869.
- [20] P. Korfiatis and B. Erickson, “Deep learning can see the unseeable: predicting molecular markers from {MRI} of brain gliomas,” *Clin. Radiol.*, vol. 74, no. 5, pp. 367–373, 2019.
- [21] J. Xu *et al.*, “Radiomics features based on MRI predict BRAF V600E mutation in pediatric low-grade gliomas: A non-invasive method for molecular diagnosis,” *Clin. Neurol. Neurosurg.*, vol. 222, p. 107478, 2022, doi: <https://doi.org/10.1016/j.clineuro.2022.107478>.
- [22] L. Zhang, D. V. Fried, X. J. Fave, L. A. Hunter, J. Yang, and L. E. Court, “IBEX: an open infrastructure software platform to facilitate collaborative work in radiomics,” *Med. Phys.*, vol. 42, no. 3, pp. 1341–1353, Mar. 2015, doi: 10.1118/1.4908210.
- [23] J. J. M. van Griethuysen *et al.*, “Computational Radiomics System to Decode the Radiographic Phenotype,” *Cancer Res.*, vol. 77, no. 21, p. e104 LP-e107, Nov. 2017, doi: 10.1158/0008-5472.CAN-17-0339.
- [24] A. Fedorov *et al.*, “3D Slicer as an image computing platform for the Quantitative Imaging Network.,” *Magn. Reson. Imaging*, vol. 30, no. 9, pp. 1323–1341, Nov. 2012, doi: 10.1016/j.mri.2012.05.001.
- [25] T. Rohlfing, N. M. Zahr, E. V. Sullivan, and A. Pfefferbaum, “The SRI24 multichannel atlas of normal adult human brain structure,” *Hum. Brain Mapp.*, vol. 31, no. 5, pp. 798–819, May 2010, doi: 10.1002/hbm.20906.
- [26] T. Ojala, M. Pietikainen, and T. Maenpaa, “Multiresolution gray-scale and rotation invariant texture classification with local binary patterns,” *IEEE Trans. Pattern Anal. Mach. Intell.*, vol. 24, no. 7, pp. 971–987, 2002, doi: 10.1109/TPAMI.2002.1017623.

- [27] M. Schmier *et al.*, “Repeatability of Multiparametric Prostate MRI Radiomics Features,” *Sci. Rep.*, vol. 9, no. 1, p. 9441, Jul. 2019, doi: 10.1038/s41598-019-45766-z.
- [28] X. Sun *et al.*, “Histogram-based normalization technique on human brain magnetic resonance images from different acquisitions,” *Biomed. Eng. Online*, vol. 14, no. 1, p. 73, 2015, doi: 10.1186/s12938-015-0064-y.
- [29] J. C. Reinhold, B. E. Dewey, A. Carass, and J. L. Prince, “Evaluating the Impact of Intensity Normalization on MR Image Synthesis,” *Proc. SPIE--the Int. Soc. Opt. Eng.*, vol. 10949, p. 109493H, Mar. 2019, doi: 10.1117/12.2513089.
- [30] S. Rahman, M. M. Rahman, M. Abdullah-Al-Wadud, G. D. Al-Quaderi, and M. Shoyaib, “An adaptive gamma correction for image enhancement,” *EURASIP J. Image Video Process.*, vol. 2016, no. 1, p. 35, 2016, doi: 10.1186/s13640-016-0138-1.
- [31] M. Kociołek, M. Strzelecki, and R. Obuchowicz, “Does image normalization and intensity resolution impact texture classification?,” *Comput. Med. Imaging Graph.*, vol. 81, p. 101716, 2020, doi: <https://doi.org/10.1016/j.compmedimag.2020.101716>.
- [32] T. Ivanics *et al.*, “A pre-tace radiomics model to predict HCC progression and recurrence in liver transplantation. a pilot study on a novel biomarker,” *J. Transplant.*, 2020.
- [33] K. Namdar, M. A. Haider, and F. Khalvati, “A Modified AUC for Training Convolutional Neural Networks: Taking Confidence Into Account,” *Front. Artif. Intell.*, vol. 4, p. 155, 2021, doi: 10.3389/frai.2021.582928.
- [34] A. Zwanenburg *et al.*, “The Image Biomarker Standardization Initiative: Standardized Quantitative Radiomics for High-Throughput Image-based Phenotyping.,” *Radiology*, vol. 295, no. 2, pp. 328–338, May 2020, doi: 10.1148/radiol.2020191145.
- [35] P. Virtanen *et al.*, “{SciPy} 1.0: Fundamental Algorithms for Scientific Computing in Python,” *Nat. Methods*, vol. 17, pp. 261–272, 2020, doi: 10.1038/s41592-019-0686-2.

Appendix A. How 2D features are extracted from 3D ROIs

When full-set feature extraction for a 3D ROI is enabled, 2D LBP features are extracted but 2D shape features are skipped by PyRadiomics. With the default settings, 2D LBPs are calculated for each slice of the ROI in the axial direction and stacked. The following code snippet from PyRadiomics shows how 2D LBP features are calculated for 3D ROIs (<https://github.com/AIM-Harvard/pyradiomics/blob/master/radiomics/imageoperations.py>).

```
lbp_radius = kwargs.get('lbp2DRadius', 1)
lbp_samples = kwargs.get('lbp2DSamples', 8)
lbp_method = kwargs.get('lbp2DMethod', 'uniform')

im_arr = sitk.GetArrayFromImage(inputImage)

Nd = inputImage.GetDimension()
if Nd == 3:
    # Warn the user if features are extracted in 3D, as this function calculates LBP in 2D
    if not kwargs.get('force2D', False):
        logger.warning('Calculating Local Binary Pattern in 2D, but extracting features in 3D.
Use with caution!')
        lbp_axis = kwargs.get('force2Ddimension', 0)

    im_arr = im_arr.swapaxes(0, lbp_axis)
    for idx in range(im_arr.shape[0]):
        im_arr[idx, ...] = local_binary_pattern(im_arr[idx, ...],
                                              P=lbp_samples,
                                              R=lbp_radius,
                                              method=lbp_method)

    im_arr = im_arr.swapaxes(0, lbp_axis)
```

Appendix B. Grid space of the RF models

Table 2. Grid space of the RF models

Hyperparameter	Grid Space
n_estimators	50, 100, 200
max_features	'auto', 'sqrt'
max_depth	None, 5, 10

Appendix C. Data management

Data management is an essential part of radiomics studies. To avoid data fragmentation and possible mistakes, we suggest saving the features, GT labels, clinical variables, and any other information in a single csv file. Each row of the csv file (except the header row) should belong to a unique ROI. For the studies where a patient might have multiple ROIs, creating unique ROI IDs and appending them as the first column to the dataset is preferred. The naming of the radiomics datasets (csv files) is important. All names start with “Radiomics”, and the format is always csv. We use ‘_’ as the separator to include type of the normalization, and sequence in the naming. If needed, other pieces of information can be included. Obviously, no underscore should be used within the parts. Two examples of naming would be Radiomics_Gamma-0.5_FLAIR.csv, and Radiomics_NoNormalization_ED_T1.csv. In this research, we study the effect of image normalization, imaging sequence, tumor subregion, and PyRadiomics settings on an adult brain tumor classification pipeline. As it was mentioned, we have 6 image normalization methods (i.e., NoNormalization,

Gamma0.5, Gamma1.5, Histogram, ZScore, and MinMax), 4 imaging sequences (T1, T1CE, T2, FLAIR), 4 tumor subregions (i.e., whole tumor, AT, ED, and NETnNCR), 3 different binWidth values (i.e., 15, 25, and 35). This creates 288 sets of tabular datasets for the radiomic features (~2.9 GB of data).

Appendix D. Other technical concerns

Although no randomness is involved in the feature extraction process, seeding is recommended in all the codes. This improves reproducibility of the results if random IDs are assigned to ROIs, or further analysis such as dimensionality reduction and data visualization are incorporated into the scripts. We encourage extracting the full set of radiomics features, which is not enabled by default (`extractor.enableAllImageTypes()` and `extractor.enableAllFeatures()` will result in a full set feature extraction).

Radiomics-based ML pipelines are more explainable compared with DL, which is a result of the transparent definitions of the radiomic features. Radiomics studies usually are concluded by highlighting the most important features, and we encourage this approach. However, not every algorithm is explainable. As an example, once an NN classifies a radiomics example, determining the influential features is perplexing. RF is an explainable model, and thus feature importances of an RF classifier can be derived. We capture the most important feature of each N experiments, for each dataset. Hence, we will have a list of $288 \times N$ top features, and the most frequent element of the list will represent the number one radiomics feature for BraTS 2020 tumor type classification. The last technical point is the choice of $N=100$ and $N_val=100$, which is made based on the practice of the Central Limit Theorem (CLT). This number of repetitions eliminates the need for k-fold cross-validation. Hence, we suggest setting N and N_vals above 30, where computational costs allow, and switching to k-fold cross-validation, otherwise.

Appendix E. Open-radiomics settings for the current research

Table 3. Open-radiomics settings for the current research

	Technical consideration	Setting for the current research
1	Sources of variability for the research must be identified	Segmentation (intra- and inter-reader variability), Imaging scanner vendor, imaging protocol, Imaging sequence, binWidth, image normalization, tumor subregion
2	The sources of variability, whose effect will be measured, should be highlighted	Imaging sequence, binWidth, image normalization, tumor subregion
3	Authors should mention which tool was used for radiomics extraction	PyRadiomics
4	It must be confirmed all the required libraries were installed	check
5	All possible features should be extracted	Check

6	It should be highlighted whether the study was 2D or 3D	3D
7	The list of the extracted radiomics feature names must be provided in the supplementary materials	Check
8	A sample of the diagnostics features must be provided in the supplementary materials	Check
9	The data split and model initialization must be repeated	yes, we employed repeated train/validation/test and set different random states for the models with each split
10	It must be highlighted if the pipeline included feature engineering	yes, the feature engineering was learned from the development set
11	The model, hyperparameter grid space, and evaluation metric(s) must be discussed in detailed	check
12	It should be highlighted if the final model was trained on the development set or the training cohort	The final models were trained on the developments sets
13	It is highly recommended the dataset (extracted radiomics features and the ground truth labels) be open-sourced	yes
14	The details of how the top-performing radiomics features were identified must be provided	We selected the top features based on RF feature importance scores

Appendix F. Feature Extraction Failure

We define the failure as a fatal error or a timeout produced by the PyRadiomics library during the feature extraction. On a system with an AMD Ryzen threadripper pro 3955wx, 128 GB of RAM, 4 TB of M2 SSD, running Ubuntu 20.04.4 LTS, we set the timeout threshold at 120 seconds which created a safe margin because common ROI feature extraction time was of the order of seconds. Corresponding figures are provided in supplemental material. It should be highlighted that identifying the reason for feature extraction failure is out of the scope of this research.

Supplemental Material

<https://drive.google.com/file/d/1VMxsuebtdnMFBjkn4uhxivzS1hPv3TNGC/view?usp=sharing>